Physica Scripta

INCLUSIVE PUBLISHING TRUSTED SCIENCE

PURPOSE-LED PUBLISHING™

PAPER • **OPEN ACCESS**

Fabrication and characterization of ZnBo-based ultrasonic transducers for potential cardiovascular sensing applications

To cite this article: Gökhan Ekinci *et al* 2026 *Phys. Scr.* **101** 435910

View the article online for updates and enhancements.

You may also like

- Quantum exciton dynamics in mesoscopic rings under magnetic fields: Aharonov–Bohm oscillations, optical response, and thermodynamic properties
Varsha and Vinod Prasad
- The Dunkl–Schrödinger equation with screened Coulomb potential: approximate bound states and the double-confluent Heun equation
Axel Schulze-Halberg
- Study on barchan dune movement velocity using fiber optic sensing theory and technology: a case study in the Tengger Desert, China
Kesen Tao, Xin Ma, Jinsheng Yu et al.

This content was downloaded from IP address 193.255.177.234 on 02/11/2026 at 01:16

Physica Scripta

Check for updates

OPEN ACCESS

RECEIVED
26 July 2026

REVISED
5 October 2026

ACCEPTED FOR PUBLICATION
16 October 2026

PUBLISHED
27 October 2026

Original content from this work may be used under the terms of the Creative Commons Attribution 4.0 licence.

Any further distribution of this work must maintain attribution to the author(s) and the title of the work, journal citation and DOI.

PAPER

Fabrication and characterization of ZnBo-based ultrasonic transducers for potential cardiovascular sensing applications

Gökhan Ekinci[1,*], **Fatih Mehmet Coşkun**[2,3] and **Sümeyye Veziroglu**[4]

[1] Department of Digital Transformation Electronics, Vocational School, Doğuş University, İstanbul 34775, Türkiye
[2] Faculty of Engineering and Natural Sciences, Department of Engineering Physics, İstanbul Medeniyet University, İstanbul, Türkiye
[3] Istanbul Medeniyet University Science and Advanced Technology Research Center (IMU-BILTAM), İstanbul, Türkiye
[4] Faculty of Science, Department of Physics, Marmara University, İstanbul, Türkiye
[*] Author to whom any correspondence should be addressed.

E-mail: gekinci@dogus.edu.tr

Keywords: ultrasonic bio-sensor, piezoelectric materials, transducer, ZnBO

Abstract

Cardiovascular diseases, driven primarily by hypertension and atherosclerosis, remain a leading cause of mortality worldwide. Long-term continuous monitoring of blood pressure waveforms is essential for early diagnosis and clinical intervention. In this study, we report the first fabrication and characterization of boron-doped zinc oxide (ZnBO)-based ultrasonic transducers designed for invasive (e.g. catheter-based) and noninvasive (e.g. external sensors) cardiovascular blood pressure measurements. Transducer devices with a Si/$Zn_{0.95-X}B_{0.05}O$/Ti/Au stack architecture were fabricated on self-oxidizing Si(100) substrates via the sol-gel dip-coating method and magnetron sputtering. The surface morphology and elemental composition of the ZnBO films were examined in detail using scanning electron microscopy and energy-dispersive x-ray analysis. In addition, the crystal structure and phase composition of the ZnBO films were analyzed using x-ray diffraction. The electrical characterization of the fabricated ZnBO-based ultrasonic transducers was performed autonomously using a LabVIEW interface under a 500 kHz sinusoidal excitation wave. The fabricated transducers generated substantial output voltages of up to +3 V and −4 V with minimal wave distortion, matching the transducer performance and −6 dB fractional bandwidth requirements demanded by advanced cardiovascular monitoring systems.

1. Introduction

High blood pressure, also known as hypertension, is the primary cause of cardiovascular diseases, which can have life-threatening consequences. Cardiovascular diseases are defined as conditions that affect the heart and blood vessels in other vital organs, leading to outcomes such as heart disease, vascular blockages, and stroke [1, 2]. According to international health studies, cardiovascular diseases account for approximately 30% of deaths worldwide, partly as a result of rapidly changing lifestyles [3]. It has been clearly observed that the vast majority of these deaths are linked to heart disease and high blood pressure, particularly stroke and coronary artery disease [4–6]. Recent studies indicate that these numbers will increase substantially, and that healthcare and treatment costs associated with these diseases will reach approximately $400 billion worldwide [7, 8]. Despite its devastating effects and the substantial costs associated with its diagnosis and treatment, hypertension control rates and awareness of its health impacts remain low worldwide [9, 10]. Changes in blood pressure waveforms can provide researchers with information for the detection and study of cardiovascular disorders, which have a dynamic nature [11–13]. Peaks in arterial blood pressure waveforms can provide information about left-sided heart events, while peaks in venous blood pressure waveforms can provide information about right-sided heart events. Continuously monitoring and analyzing these subtle changes in waveforms can lead to significant advances in the diagnosis and treatment of hypertension and cardiovascular diseases

© 2026 The Author(s). Published by IOP Publishing Ltd

[14–17]. Throughout history, various invasive and noninvasive imaging techniques have been developed to both measure high blood pressure and comprehensively examine the structure of atherosclerotic plaques [13, 14]. Compared to invasive methods, noninvasive blood pressure measurement is more reliable, faster, and, most importantly, requires less expertise [18–20]. However, invasive methods, particularly intravascular ultrasound imaging, provide more comprehensive information in the evaluation of the coronary artery and in the more precise examination of abnormalities within it [17, 21]. At this point, ultrasonic waves stand out with their ability to penetrate to sufficient depths for both invasive and noninvasive methods. Thus, based on the ability of ultrasonic waves to penetrate tissues, biocompatible, state-of-the-art ultrasonic transducers can provide continuous temporal dynamics without interruption of communication with the skin and tissue surface. Undoubtedly, continuous and precise monitoring of deep biological tissues and organs will open the door to new radical changes in the diagnosis and treatment of cardiovascular diseases [14, 22, 23]. A conceptual illustration of the potential application of ultrasonic sensing in cardiovascular monitoring is provided in figure 1.

Recent advances in ultrasonic transducers have focused on miniaturized, flexible, and wearable platforms that integrate advanced piezoelectric materials and acoustic transducers for real-time, noninvasive, and continuous physiological monitoring [24–26]. In parallel, acoustic-wave biosensing technologies such as QCM, FBAR, SAW, and acoustofluidic platforms are increasingly being integrated with microfluidics to enable sensitive, label-free, and point-of-care detection of biological analytes [27, 28]. Current research is therefore moving toward highly integrated systems combining flexible piezoelectric transducers, microfluidics, wireless electronics, and multimodal signal analysis for continuous biomedical monitoring and personalized healthcare [29, 30]. Studies show that ultrasonic transducers can be manufactured using various piezoelectric structures with perovskite architecture, such as ZnO, ZrO_2, BN, BT, ceramic materials, AlN, and PZT-4, PZT-8, $BiScO_3$-$PbTiO_3$-Co, and $BaTiO_3$-$CaTiO_3$-Co [31–35]. Among these compounds, ZnO is a highly promising material due to its high piezoelectric strain constant, high biocompatibility, and wide bandgap, which makes it suitable for optoelectronic applications [36–39]. ZnO is an attractive piezoelectric material owing to its non-centrosymmetric wurtzite crystal structure, which enables efficient electromechanical transduction, while its wide band gap, good mechanical properties, and compatibility with thin-film and nanostructure fabrication provide additional advantages for sensor applications [40, 41]. Furthermore, ZnO offers relatively low-cost processing, biocompatibility, and a high surface-to-volume ratio, while its high isoelectric point facilitates biomolecule immobilization, making it particularly attractive for piezoelectric biosensing applications [42, 43]. Additionally, ZnO piezoelectric materials with a high piezoelectric coefficient can be fabricated on various substrates and require a low epitaxial growth temperature compared to other piezoelectric counterparts. This low epitaxial growth temperature ensures that they possess a stoichiometry and texture that are easier to control during production. All these properties make this compound a viable candidate for use as an acoustoelectric conversion layer in ultrasonic applications [32, 44]. Recent studies highlight that boron-doped ultrasonic sensors possess intrinsic polarization driven by the polar nature of the B–O bond, thereby exhibiting exceptional piezoelectric properties. Due to this polarization effect, their performance transcends that of conventional piezoelectric polymers and rivals the superb characteristics of wurtzite semiconductors [34, 45]. Boron doping is expected to modify the ZnO lattice through the incorporation of B into the ZnO crystal structure, thereby inducing lattice distortion, defects, and changes in carrier concentration that can influence electromechanical coupling and piezoelectric response [46, 47]. Recent studies on doped ZnO demonstrate that controlled doping can tailor lattice structure, defect states, and carrier concentration, providing a pathway toward enhanced piezoelectric and sensing performance; therefore, B doping may offer a route to optimize the electromechanical response of ZnO-based biosensors [48]. Driven by these superior attributes, this study utilizes a functional zinc-boron oxide (ZnBO) framework as the piezoelectric layer instead of pristine zinc oxide (ZnO). The incorporation of boron atoms into the zinc lattice—either substitutionally or interstitially—induces a localized lattice distortion. This distortion drastically enhances the intrinsic dipole moment and remanent polarization compared to pure ZnO. Given that the sensor mechanism relies on a piezoelectric polarization-based transducer, this lattice deformation directly amplifies the signal sensitivity [49–51]. Furthermore, boron exhibits a high chemical binding energy, with the B–O bond being significantly stronger than the Zn–O bond. Incorporating boron suppresses the formation of uncontrolled oxygen vacancies and imparts a more robust chemical stability to the material; this effectively stabilizes the sensor, mitigates background noise, and yields a higher signal-to-noise ratio (SNR) [52, 53]. Compared with conventional piezoelectric materials such as PZT and AlN, ZnBO (boron-doped ZnO) offers a lead-free, biocompatible and readily tunable platform in which boron doping can modify the electrical properties and piezoelectric response of ZnO, making it particularly attractive for ultrasonic biosensing applications [46]. Additionally, boron

acts as an n-type donor within the ZnO matrix or modulates the conduction mechanism via the formation of borate phases, thereby optimizing the interfacial charge transfer resistance at the transducer interface. While pristine ZnO often suffers from extreme conductivity or excessive insulation, the synthesized ZnBO phase provides an optimal charge carrier concentration tailored for high-performance sensor operation [54–56]. Accordingly, the main research question addressed in this study is whether boron incorporation into ZnO can improve its ultrasonic transduction performance compared with pristine ZnO. To address this question, we fabricate ZnBO-based ultrasonic transducers using a low-temperature-compatible sol-gel dip-coating approach and systematically characterize their structural, morphological, elemental, and acoustic properties. In particular, this study aims to investigate the effect of ZnBO film thickness on device characteristics and to compare the acoustic response of ZnBO and undoped ZnO devices, with the objective of evaluating the potential of ZnBO thin films as a lead-free piezoelectric platform for future cardiovascular sensing applications.

2. Experimental details

In this study, transducer devices with a stack structure of Si/$Zn_{0.95-X}B_{0.05}O$/Ti/Au were grown in thin film form using the sol-gel method and the DC magnetron sputtering. The 5% B concentration was selected as a moderate doping level to promote the incorporation of B into the ZnO lattice while preserving the hexagonal wurtzite ZnO framework and minimizing the possibility of secondary boron-containing phases, which could obscure the specific contribution of B doping to the ultrasonic response [57]. After chemical and thermal cleaning of commercially available and self-oxidizing Si(100) substrates, ZnBO thin film structures were grown onto the substrates by the sol-gel method with 1, 2, 3, and 20 coating cycles. These Si/$Zn_{0.95-x}B_{0.05}O$ thin films were synthesized by the sol-gel method under carefully controlled conditions. Zinc acetate dihydrate ($Zn(CH_3COO)_2 \cdot 2\ H_2O$) and boric acid ($H_3BO_3$) were used as metal precursors, methanol (CH_3OH) as solvent, and monoethanolamine (MEA, C_2H_7NO) as stabilizer. All chemicals were of analytical grade with purity above 99%. To obtain the desired stoichiometric composition, the precursor materials were precisely weighed using an analytical balance, ensuring a total metal ion concentration of 0.25 M. The weighed precursors were placed in glass beakers containing Teflon-coated magnetic stirring rods. Then, 40 ml of methanol and approximately 7.5×10^{-1} ml of MEA were added to the mixture. To minimize solvent evaporation during the preparation process, the beakers were sealed with Parafilm. The solutions were then magnetically stirred at 300 rpm for 24 h at room temperature to obtain transparent and homogeneous precursor solutions suitable for thin film coating. To achieve a clean, smooth, and homogeneous surface, the substrates underwent a multi-step cleaning process. First, the silicon substrates were washed with a detergent solution to remove surface contaminants such as oil and organic residues, and then thoroughly rinsed with deionized water. The substrates were then immersed in methanol to further enhance surface cleanliness, and subsequently dried using a drying device. This cleaning process was repeated several times until the silicon substrates were completely free of visible contaminants. After the cleaning process, the substrates were placed vertically in the coating assembly, and the coating process commenced. The thin film coating process was performed using a dip coating system. Cleaned substrates were dipped into and removed from precursor solutions at a constant withdrawal rate to ensure a homogeneous coating across the entire surface. The coating process was carried out using a layer-by-layer approach. After each coating step, the samples were preheated in a vertical oven at 400 °C for 120 s to remove residual solvent and initiate the decomposition of the precursor. Following this step, the films were allowed to cool at room temperature for 180 s before applying the next layer. The Si/ZnBO structures were prepared by repeating the coating cycle 1, 2, 3, and 20 times, obtaining structures of different thicknesses. This approach allowed for the systematic investigation of the effect of film thickness on material properties. Finally, to obtain the crystalline wurtzite phase, all deposited films were thermally treated at 600 °C for 30 min under ambient atmospheric conditions. Based on our previous laboratory experience and preliminary optimization experiments on sol-gel-derived ZnO thin films, a calcination temperature of 600 °C was selected as the optimized condition for obtaining the crystalline hexagonal wurtzite ZnO phase while maintaining good film quality and reproducibility. After heat treatment, 100-nm-thick Ti and 30-nm-thick Au electrical contact layers were deposited on Si/ZnBO structures using a magnetic sputtering system in a high vacuum environment. The Ti/Au thicknesses were selected based on our previous device fabrication experience, with the 100 nm Ti layer serving primarily as an adhesion and mechanically stable interfacial layer, while the 30 nm Au layer provides a continuous, low-resistance conductive electrode for reliable electrical and ultrasonic measurements. As schematically shown in figure 2, a metallic mask was used

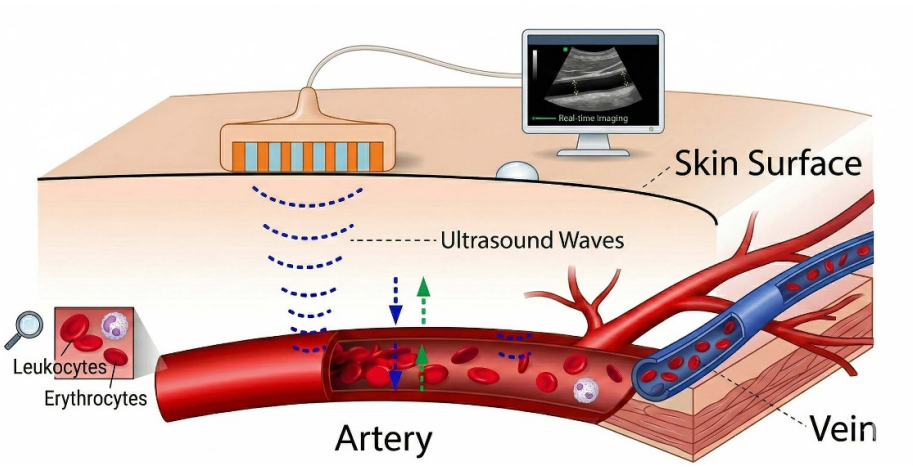


Figure 1. Conceptual illustration of the potential application of ultrasonic sensing for cardiovascular monitoring.

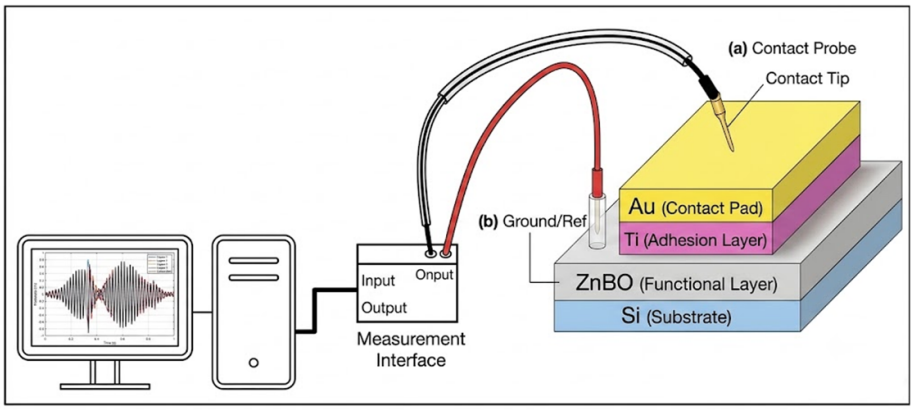


Figure 2. Schematic representation of the fabricated ZnBO-based ultrasonic transducer and experimental electrical measurement configuration.

to provide electrical contact over the ZnBO. The electrodes have an approximately rectangular geometry, defining an active device area of approximately 1 mm^2. The structural characterization of the piezoelectric ZnBO layer in the device structure was performed in detail. For this purpose, x-ray diffraction analysis (XRD) was performed to investigate the crystal structure of this layer. A Rigaku XRD instrument with a CuKα x-ray source ($\lambda = 0.154$ nm) was used for XRD measurements. To determine the surface morphology and thickness of the ZnBO structure, surface analysis and cross-sectional measurements were also performed using Scanning Electron Microscopy (SEM). Furthermore, Energy Dispersive x-ray Analysis (EDX) measurements were carried out for elemental analysis and chemical characterization of the ZnBO film structure. Electrical acoustic measurements were performed to demonstrate that the devices function as ultrasonic transducers. In the electrical characterizations, the ZnBO portion was always grounded, and sinusoidal waves at a frequency of 500 kHz were sent to these portions using a National Instruments function generator controlled via LabVIEW. To read the waves from the ZnBO portion, an oscilloscope, also supported by LabVIEW National Instruments, was connected to the upper electrodes. All the acoustic measurements were performed in air at room temperature, without the use of a liquid medium or tissue phantom, and with measurement setups created using the LabVIEW software interface.

3. Results and discussion

Cross-sectional SEM analyses revealed that the thicknesses of ZnBO thin films produced with 1, 2, 3, and 20 coating cycles were 17, 40, 55, and 207 nm, respectively. Figure 3 shows the SEM surface morphologies of ZnBO thin films with different immersion numbers, i.e. different thicknesses. These SEM

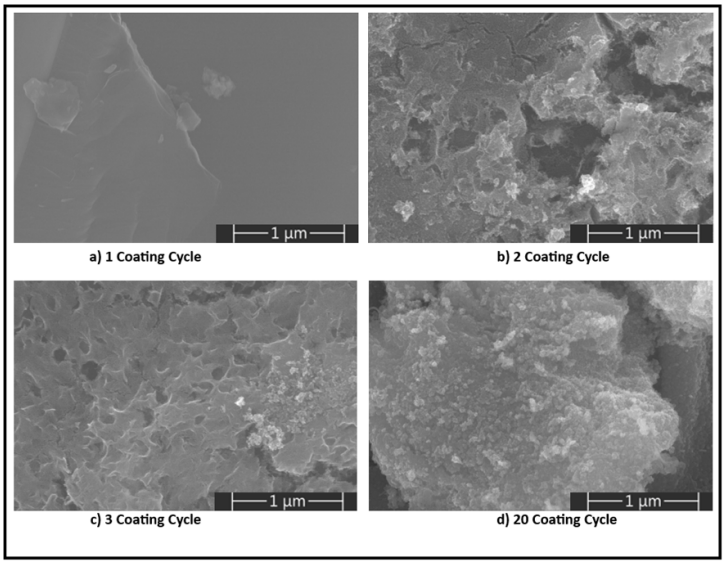


Figure 3. SEM images of ZnBO Films.

images clearly show that the surface morphologies of ZnBO thin films change with increasing thickness. The surface morphology of the film with an immersion number of 1 is different from the others, and no dense structure is observed on the surface. However, the surface morphologies of ZnBO films with immersion numbers of 2, 3, and 20 have transformed into variable-sized nanoparticles with increasing thickness. While the morphology of ZnBO films with immersion numbers of 2 and 3 is in the form of an overlapping network, the surface morphology of the ZnBO film with an immersion number of 20 is entirely in the form of variable-sized nanoparticles. Furthermore, while the morphology of ZnBO films with immersion numbers 2 and 3 shows very little aggregation, the surface morphology of the ZnBO film with immersion number 20 shows more intense aggregation. In general, no defects were observed on the film surfaces; only denser surface structures were obtained with increasing film thickness.

The elemental composition of ZnBO thin films prepared with different coating cycles was investigated using EDX analysis. Figures 4–7 show the EDX spectra and elemental distributions of ZnBO thin film structures. The intensity of the Si peak originating from the substrate is highest for the film with 1 coating cycle, decreases as the number of cycles increases, and reaches a minimum at 20 cycles. This trend clearly shows that the thickness of ZnBO thin films increases with coating cycles, thus weakening the substrate signal. The Zn content was lowest after one coating cycle and gradually increased, reaching a maximum at 20 cycles. In contrast, the oxygen (O) content remained relatively stable as the number of coating cycles increased compared to the Zn element. This stable behavior is attributed to the inevitable oxidation processes during the characterization stages carried out under ambient atmospheric conditions. Due to the low atomic number of boron (B) and its relatively low presence in the film structure, its detected concentration remained relatively low compared with those of the other elements in the EDX spectra. These elemental data provide significant evidence for the formation of Zn–O and B–O chemical bonds, confirming the successful establishment of the ZnBO network structure. Additionally, trace amounts of carbon (C) were detected, attributable to unavoidable environmental contamination during the production or characterization phases. No other impurity elements were observed in the EDX spectra. Consistent with SEM analyses, the highest percentage of zinc was recorded for the film produced with 20 coating cycles, exhibiting the densest surface morphology. Overall, the EDX findings confirm the successful and desired growth of ZnBO thin films for all coating cycles.

The crystal structures of the synthesized ZnBO thin films, developed for transducer device fabrication, were investigated using XRD. The XRD patterns revealed characteristic diffraction peaks corresponding to ZnO and metallic Zn phases within the ZnBO matrix. Figure 8 illustrates the XRD profiles of the films deposited on Si substrates across various coating cycles. All synthesized ZnBO thin films exhibited a crystalline nature, displaying distinct reflections corresponding to the (100), (002), (101), (102), (110), and (103) lattice planes of ZnO. A dominant preferential orientation along the (101) plane was observed for all samples, confirming the growth of crystalline ZnO thin films with a hexagonal wurtzite structure. The peak positions and relative intensities are in excellent agreement with the JCPDS Card No. 36–1451 [58, 59]. Furthermore, a characteristic peak associated with the (101) plane

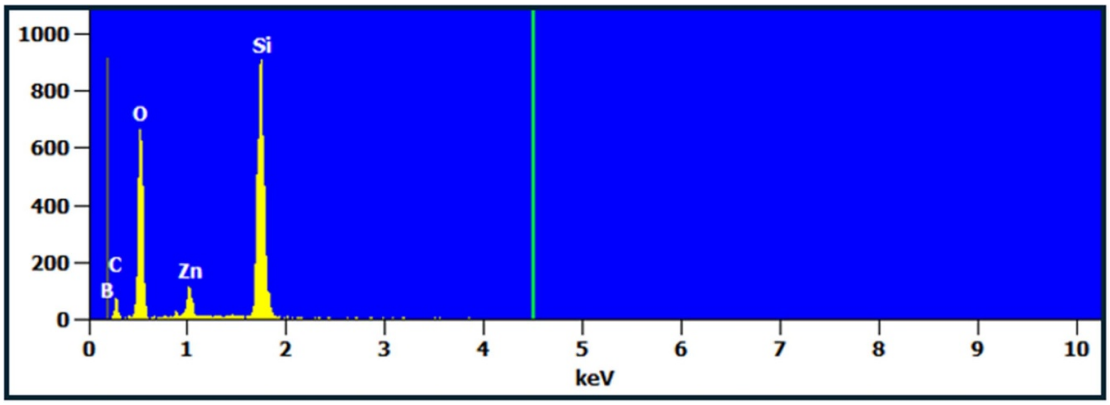


Figure 4. EDX spectra of 1- coating cycle ZnBO thin film.

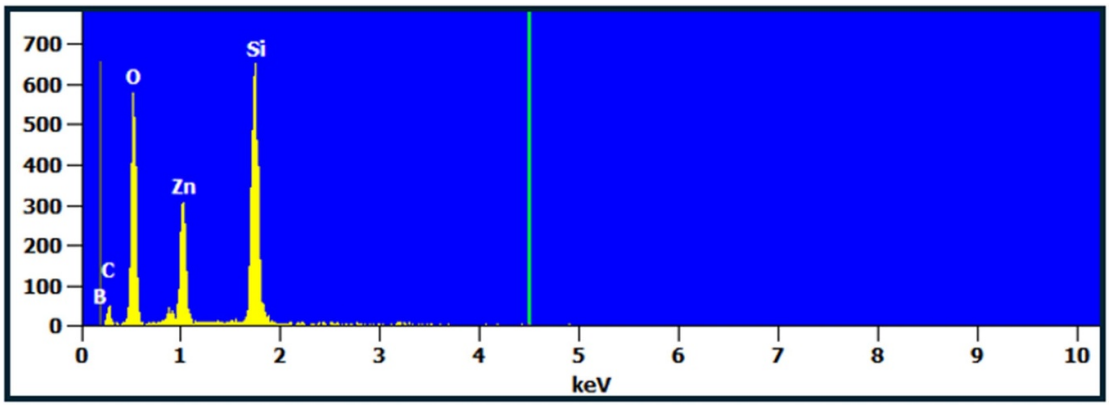


Figure 5. EDX spectra of a 2-coating-cycle ZnBO thin film.

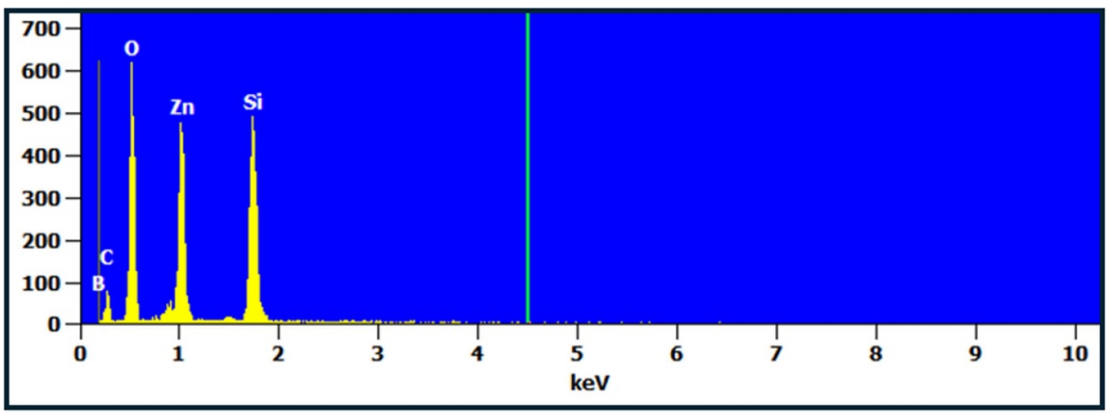


Figure 6. EDX spectra of a 3-coating-cycle ZnBO thin film.

of metallic Zn was detected in the films deposited with 1, 2, and 3 coating cycles [60]. The presence of this metallic Zn phase in the initial cycles (1–3) and its subsequent disappearance at 20 cycles can be elucidated by the activation energy required for complete crystallization. Consistent with the mechanism proposed by Weverton *et al* [60], the limited film thickness during the initial three cycles might have prevented the system from acquiring sufficient thermal/kinetic energy to overcome the crystallization barrier. Consequently, a portion of the precursor zinc remained in its metallic state while the rest oxidized into ZnO. With increasing coating cycles, the characteristic diffraction peak associated with metallic Zn progressively decreases in intensity. At 20 coating cycles, this peak is no longer detectable within the XRD detection limit, indicating a substantial reduction of the metallic Zn phase contribution. This

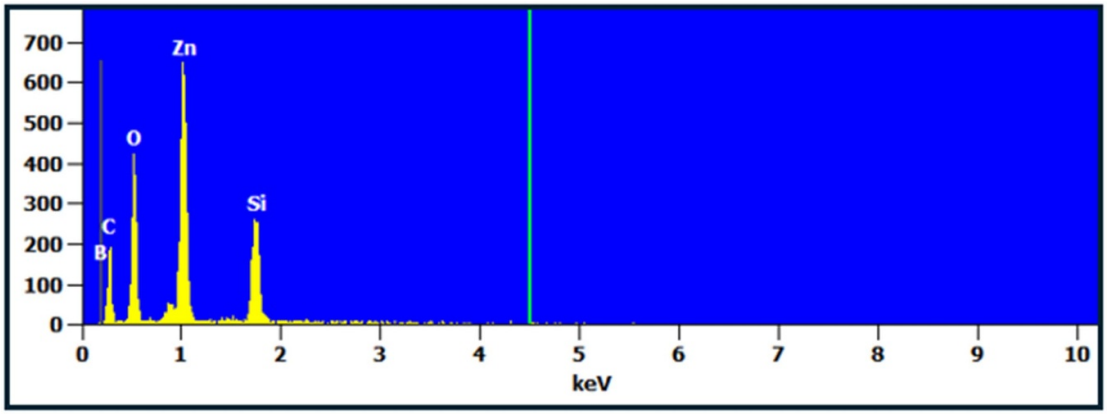


Figure 7. EDX spectra of a 20-coating-cycle ZnBO thin film.

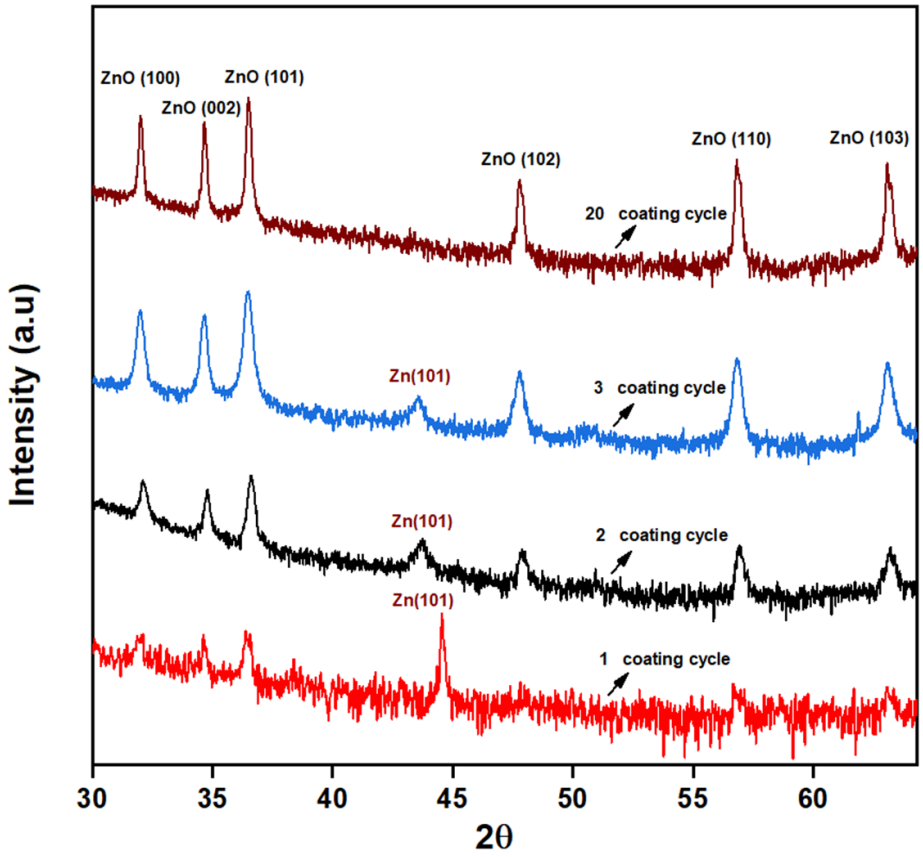


Figure 8. XRD spectra of ZnBO thin films.

behavior suggests that increasing the coating thickness and the associated thermal treatment promote the conversion of the initially metallic Zn-containing phase toward the oxide/borate phase observed in the final film. Additionally, as the film thickness increased with the number of coating cycles, the diffraction peaks of ZnO became progressively sharper and more intense, indicating an improvement in crystallinity and grain size (e.g. transitioning from the relatively broad peaks of the 1-cycle film to the highly intense, well-defined reflections of the 20-cycle film). Furthermore, no characteristic diffraction peaks corresponding to boron (B) or boron-related phases were observed in any of the XRD patterns. This absence can be attributed to the extremely low doping concentration of boron and its low atomic number, which significantly reduces its x-ray scattering factor, rendering it below the detection limit of conventional XRD analysis [61].

The fabricated ultrasonic transducers were characterized by acoustic measurements. These acoustic measurements were performed autonomously using the LabVIEW software interface supported by

National Instruments. Under these conditions, stimulating sinusoidal waves with a frequency of 500 kHz and a peak-to-peak voltage of 3 V (V_{pp}) were sent to the ultrasonic transducers, as shown in figure 9. Considering the thickness and acoustic characteristics of the ZnBO layer, the fundamental acoustic resonance of the fabricated structure is estimated to be in the sub-MHz to MHz frequency range. Accordingly, a 500 kHz sinusoidal excitation was selected as a practical operating frequency to efficiently stimulate the acoustic response of the ZnBO-based sensor. This frequency was chosen to provide a stable and reproducible acoustic excitation during the measurements. The ZnBO-based sensors were experimentally investigated at frequencies up to 500 kHz. Since a systematic frequency-response characterization was not performed, 500 kHz should be regarded as the highest frequency investigated in the present study rather than as the upper limit of the sensor's usable frequency range. Determination of the complete operational bandwidth and resonance frequency requires a dedicated frequency-sweep study. The acoustic responses of the devices are given in figure 10. Furthermore, to demonstrate the effect of boron doping, figure 9 presents the acoustic response of the ZnO biosensor without boron doping. The graphs obtained for the ZnO devices show the responses of the devices under stimulating acoustic waves corresponding to ultrasonic vibrations at specific sound levels. The resulting graphs show that the devices can produce output voltages of up to +3 V and −4 V. These output voltages are quite significant, as they exceed the sensing voltage required by the most advanced neural stimulation circuits. In this way, the high output voltages obtained provide an enhanced transducer effect for users in hearing-based applications [62]. The output voltage values obtained in this study are quite consistent with the values in the literature [63]. Although ZnBO film thickness can influence the piezoelectric response, no pronounced thickness-dependent trend was observed in the output voltage within the thickness range investigated in this study. The small variations observed between the samples may arise from differences in film microstructure, crystallographic orientation, electrode/film interfaces, acoustic coupling, and experimental conditions. Therefore, the present results suggest that the thickness effect is not dominant within the investigated range; however, a broader thickness study with controlled microstructural characteristics would be required to establish the quantitative dependence of the piezoelectric response on ZnBO thickness. Based on the working mechanism of acoustic sensors, the output acoustic wave values are expected to be close to the excitation wave values, and the output voltage values in the acoustic sensors we produced are also close to the excitation voltage values [64]. When the obtained graphs were examined in terms of waveforms, it was observed that the response waveforms were quite close to the excitation waveforms and that no symmetrical distortion occurred. The graphs show that the fabricated sensors caused very little distortion in the acoustic signal. These findings demonstrate that ultrasonic conversion is performed with very good efficiency using the fabricated devices. Positive and negative peak values were determined with high accuracy; we believe this is due to the crystal structure of the film, film homogeneity, and B-doping. However, when we look at the acoustic signal obtained from the ZnO-based sensor, we clearly observed that the response waveform does not resemble the excitation waveform and that symmetrical distortion occurs. This shows that devices produced with low thicknesses using only a ZnO piezoelectric layer cannot perform ultrasonic conversion with very good efficiency. In addition, devices with a ZnBO piezoelectric active layer structure were tested without problems up to 500 kHz and demonstrated their ability to operate reliably at this frequency. The response graphs of all fabricated acoustic transducers, despite their very low thickness, resemble the typical echo response of a transducer. We believe this is achieved thanks to the B doping in the ZnBO structure used as a piezoelectric layer and the high piezoelectric efficiency of ZnO. Furthermore, we can say that the ultrasonic transducers, which also function as an effective transducer mechanism, have a very high electromechanical coupling coefficient (K_{eff}) due to their high transducer efficiencies. The pulse echo responses obtained for the fabricated devices correspond to a center frequency and fractional bandwidth of −6 dB. The obtained center frequency and fractional bandwidth of −6 dB are in very good agreement with studies in the literature [2]. Overall, it is clearly understood that the ZnO structure used as a piezoelectric active layer functions as a good ultrasonic transducer even at very low thicknesses below 100 nm. This is attributed to the superior optoelectronic and piezoelectric properties of ZnO and the improvement of piezoelectric properties by providing a polar structure through B doping. All acoustic characterization results show that the fabricated transducer transducers have a sufficient fractional bandwidth of −6 dB and adequate sensitivity for blood pressure monitoring applications. It should be noted that the present measurements demonstrate the voltage response of the ZnBO-based device under the applied acoustic excitation conditions; however, a calibrated acoustic-pressure reference was not employed. Therefore, absolute sensitivity, linearity, and hysteresis with respect to acoustic pressure could not be quantitatively determined in the present study. These parameters will be investigated in future work using a calibrated acoustic source

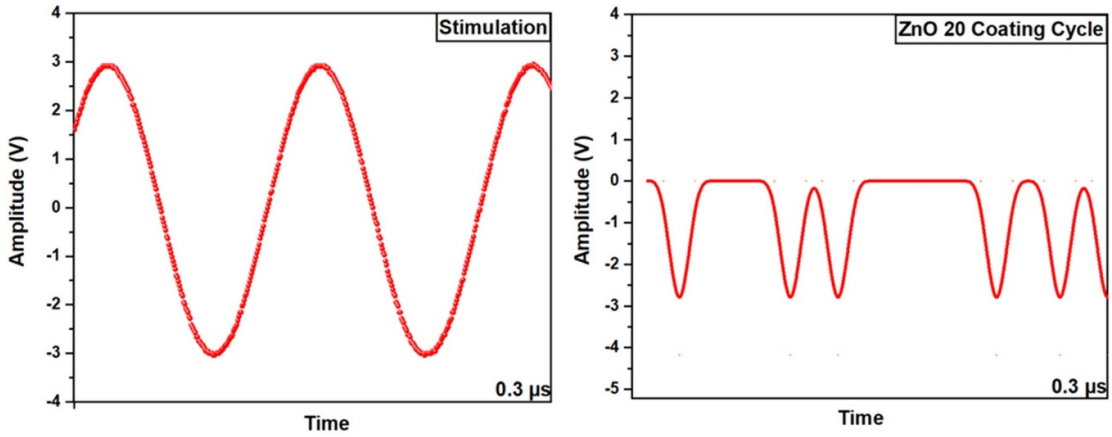


Figure 9. Stimulation pulse and the measured pulse echo impulse response of the ZnO thin film-based sensor.

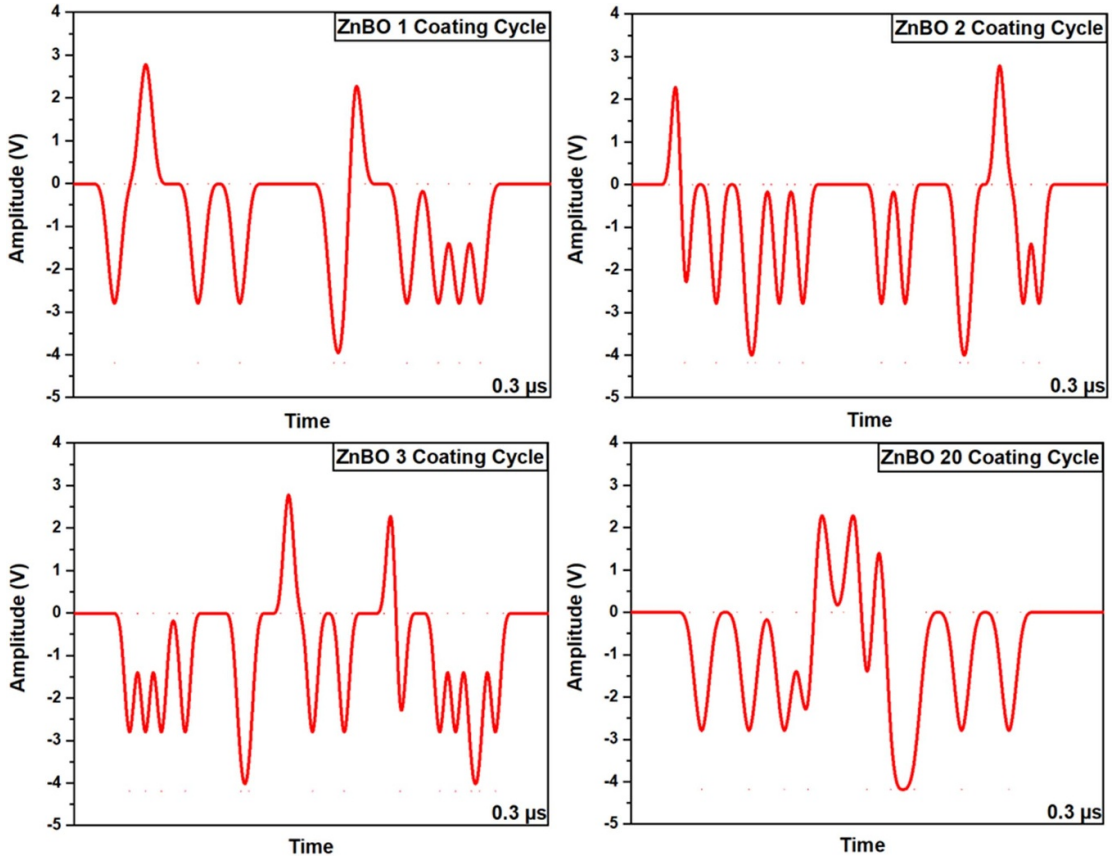


Figure 10. The measured pulse echo impulse response of the ZnBO thin film-based sensors.

and/or reference pressure sensor. All measurements in the present study were performed at room temperature. Although these experiments demonstrate the acoustic/electrical response of the ZnBO-based sensor, the effect of physiological temperature was not investigated. Since temperature can influence the electrical, mechanical, and piezoelectric properties of the sensing layer as well as acoustic coupling, the response at approximately body temperature (37 °C) may differ from the room-temperature results. The obtained electrical response demonstrates the capability of the ZnBO-based device to transduce ultrasonic excitation into a measurable electrical signal. Although this response indicates potential for pressure-related biomedical sensing, a direct quantitative relationship between the sensor output voltage and blood pressure was not established in the present study. Such a relationship requires simultaneous measurements with a calibrated blood-pressure reference system and controlled pressure variations, which will be addressed in future work.

4. Conclusions

SEM analyses revealed that the surface microstructures of piezoelectrically active ZnBO thin films changed significantly with thickness and transformed into variable-sized nanoparticles. Furthermore, SEM analyses showed that no defects formed on the surface of the ZnBO films used as piezoelectrically active layers, indicating completely homogeneous surfaces. EDX spectra showed that the ZnBO structure was successfully formed and that the thickness of the ZnBO thin films increased with increasing coating cycle number, accompanied by a decrease in the substrate-induced Si peak. Due to its low atomic number and relatively low presence in the film structure, boron exhibited a very low relative concentratio in the EDX spectra compared to other components. All elemental data obtained provide significant evidence for the formation of Zn–O and B–O chemical bonds, demonstrating the successful formation of the ZnBO bond structure. No other impurity elements were observed in the EDX spectra. It was observed that all ZnBO thin films had a crystalline structure, and crystalline ZnO thin films with a hexagonal wurtzite structure were obtained. The films exhibited characteristic diffraction peaks corresponding to the lattice planes (100), (002), (101), (102), (110), and (103) of ZnO. A dominant preferential orientation along the lattice plane (101) was observed in all samples. As the thickness of the thin films increased with respect to the number of coating cycles, the ZnO diffraction peaks in the XRD pattern gradually became sharper and more intense. This indicates that the crystal quality of the material increased and the grain size grew as the number of cycles increases. As a result of acoustic-electrical measurements, it was determined that the sensors could produce quite high output voltages reaching $+3$ V and -4 V. These voltage values are high enough to exceed the detection thresholds required by advanced neural stimulation circuits and are consistent with the values in the literature. No significant difference was observed between the output voltage values of ZnBO sensors produced with different coating cycles (different thicknesses). It was confirmed that the material functions as an extremely efficient ultrasonic transducer even at very low film thicknesses. Analysis of the obtained response waveforms revealed that the output signal was almost identical to the stimulating signal, and no symmetrical distortion occurred. The devices demonstrated highly efficient ultrasonic conversion and cause very little distortion on the acoustic signal. To confirm the success of boron doping, a comparison with a pure ZnO sensor clearly showed that the acoustic signal from the pure ZnO sensor did not resemble the stimulating wave and underwent symmetrical distortion. The improved waveform characteristics observed in the ZnBO-based devices, compared with the undoped ZnO device, suggest that boron incorporation may influence the acoustic-to-electrical transduction behavior of the ZnO-based structure. This improvement may be associated with boron-induced modifications in the lattice structure, defect states, and charge carrier concentration, as suggested by previous studies. However, since the intrinsic piezoelectric coefficients were not directly measured in the present study, further quantitative investigations are required to establish the specific contribution of boron doping to the piezoelectric performance. The high ultrasonic conversion efficiency, acoustic response, and favorable microstructural characteristics exhibited by the ZnBO thin films, even at low thicknesses, together with the flexibility of the polymer substrates and the mechanical tolerance of ZnO-based nanostructures, demonstrate the potential of the developed structure as a promising technological basis for the future development of wearable and implantable ultrasonic biosensor platforms and neural stimulation systems. However, the present study is limited to laboratory-based acoustic and electrical characterization. Future work will therefore focus on (i) performing calibrated acoustic-pressure measurements to quantitatively determine the sensitivity and linearity of the sensor, (ii) establishing a direct and quantitative correlation between the sensor output and blood pressure under controlled pressure variations, (iii) investigating sensor performance under physiologically relevant temperature conditions, (iv) evaluating the biocompatibility and long-term stability of the ZnBO thin-film structure, and (v) conducting *in vivo* studies to assess the feasibility of the proposed sensor for biomedical applications. These studies will provide the necessary experimental validation for evaluating the potential of ZnBO-based ultrasonic sensors in wearable and implantable cardiovascular sensing applications.

Data availability statement

All data that support the findings of this study are included within the article (and any supplementary files).

ORCID iD

Gökhan Ekinci 0000-0003-1918-1553

References

[1] Peng C, Wu H, Kim S, Dai X and Jiang X 2021 Recent advances in transducers for intravascular ultrasound (IVUS) Imaging *Sensors* **21** 3540
[2] Peng C, Chen M, Sim H K, Zhu Y and Jiang X 2021 Noninvasive and nonocclusive blood pressure monitoring via a flexible piezo-composite ultrasonic sensor *IEEE Sens. J.* **21** 2642–50
[3] Martin S S *et al* 2025 Heart disease and stroke statistics: a report of US and global data from the American Heart Association *Circulation* **151** 41–660
[4] Mensah G A *et al* 2017 Decline in Cardiovascular Mortality *Circ. Res.* **120** 366–80
[5] Stefanadis C, Antoniou C, Tsiachris D and Pietri P 2017 Coronary atherosclerotic vulnerable plaque: current perspectives *J. Am. Heart Assoc.* **6** e005543
[6] Arima H, Barzi F and Chalmers J 2011 Mortality patterns in hypertension *J. Hypertens* **29** S3–S7
[7] Gaziano T A, Bitton A, Anand S and Weinstein M C 2009 The global cost of nonoptimal blood pressure *J. Hypertens* **27** 1472–7
[8] Benjamin E J *et al* 2017 Heart disease and stroke Statistics—2017 update: a report from the American Heart Association *Circulation* **135** 146-603
[9] Beaglehole R 2005 Global strategies to prevent chronic diseases *S. Afr. J. Clin. Nutr.* **18** 101–5
[10] Waxman A 2003 Prevention of chronic diseases: WHO global strategy on diet, physical activity and health *Food Nutr. Bull.* **24** 281–4
[11] Chowdhury A H, Jafarizadeh B, Baboukani A R, Pala N and Wang C 2023 Monitoring and analysis of cardiovascular pulse waveforms using flexible capacitive and piezoresistive pressure sensors and machine learning perspective *Biosens. Bioelectron.* **237** 115449
[12] Xu L, Li Z, Xia P, Zhang C, Du L, Tian W and Fang Z 2026 Blood pressure estimation through pulse wave analysis using features extracted from carotid diameter distension waveforms *Biosensors* **16** 151
[13] Wu H, Tang Y, Kim H, Yao J and Jiang X 2020 Fiber based laser ultrasound transducer for intravascular thrombolysis with detective photoacoustic imaging *2020 IEEE Int. Ultrasonics Symp.* (IEEE) pp 1–4
[14] Wang C *et al* 2018 Monitoring of the central blood pressure waveform via a conformal ultrasonic device *Nat. Biomed. Eng.* **2** 687–95
[15] Mukkamala R and Xu D 2010 Continuous and less invasive central hemodynamic monitoring by blood pressure waveform analysis *Am. J. Physiol. Heart Circ. Physiol.* **299** H584–99
[16] Poznyak A V, Sadykhov N K, Kartuesov A G, Borisov E E, Melnichenko A A, Grechko A V and Orekhov A N 2022 Hypertension as a risk factor for atherosclerosis: cardiovascular risk assessment *Front. Cardiovasc. Med.* **9**
[17] Athaya T and Choi S 2022 A review of noninvasive methodologies to estimate the blood pressure waveform *Sensors* **22** 3953
[18] Hashemi S *et al* 2025 Ultra-sensitive wireless capacitive nanocomposite-based pressure sensors for health monitoring *Adv. Mater. Technol.* **10** e01316
[19] Mahdi M, Boudissa R, Laribi I, Chafia B and Imadeddine B 2025 *The Design of Piezoelectric Cantilever for Blood Sensor Device* (Sensors and Microsystems) pp 203–8
[20] Liu J, Chen D, Wang P, Song G, Zhang X, Li Z, Wang Y, Wang J and Yang J 2020 A microfabricated thickness shear mode electroacoustic resonator for the label-free detection of cardiac troponin in serum *Talanta* **215** 120890
[21] Jedrzejewski D, McFarlane E, Lacy P S and Williams B 2021 Pulse wave calibration and implications for blood pressure measurement: systematic review and meta-analysis *Hypertension* **78** 360–71
[22] Zhou Q, Lam K H, Zheng H, Qiu W and Shung K K 2014 Piezoelectric single crystal ultrasonic transducers for biomedical applications *Prog. Mater. Sci.* **66** 87–111
[23] Fu Y Q *et al* 2017 Advances in piezoelectric thin films for acoustic biosensors, acoustofluidics and lab-on-chip applications *Prog. Mater. Sci.* **89** 31–91
[24] Li J, Li G, Ma C, Li W, Yu G, Xiang L and Yao G 2026 Flexible bioelectronic sensors promote the advancement of wearable ultrasound technology in the medicine *Microsyst. Nanoeng.* **12** 244
[25] Fang M, Yu R, Meng F, Liu X, Tang N, Yuan M, Wang K and Guo J 2025 Wearable ultrasound technology in health monitoring and therapy: technological innovations, differentiated applications, and future directions *ACS Sens.* **10** 5433–55
[26] Yu X, Liang Z, Yu C, Tang Y, Chen L, Xu T, Li S, Zhang T and Huo F 2025 Recent progress of flexible and wearable ultrasound electronics: fabrication techniques and applications in healthcare *J. Mater. Chem. C* **13** 22953–72
[27] Chen C-J, Kwon J-S and Chuang H-S 2026 Acoustofluidic Biosensors *Micromachines* **17** 561
[28] Zhao Y, Parlak Z, Yu W, French D, Aquino W and Zauscher S 2024 Microfluidic QCM enables ultrahigh Q-factor: a new paradigm for in-liquid gravimetric sensing *Microsyst. Nanoeng.* **10** 116
[29] Suryaprabha T, Choi C, Wu Y, Liu L and Hwang B 2026 Smart wearable and implantable biosensors for continuous health monitoring: materials, biocompatibility, and AI integration *npj Flex. Electron.* **10** 46
[30] Zhang X *et al* 2026 Wearable ultrasound: recent advances and applications in biomedical engineering *EngMedicine* **3** 100134
[31] Barabanenkov Y N, Ivanov V V, Ivanov S N, Taranov A V and Khazanov E N 2001 Investigation of nanoceramics based on aluminum and zirconium oxides using the heat pulse method *J. Exp. Theor. Phys.* **92** 474–9
[32] Zhang Y, Jiang Y, Ma C, Zhang J and Yang B 2023 Preparation of ZnO piezoelectric thin-film material for ultrasonic transducers applied in bolt stress measurement *Coatings* **13** 1538
[33] Lee H, Zhang S, Bar-Cohen Y and Sherrit S 2014 High temperature, high power piezoelectric composite transducers *Sensors* **14** 14526–52
[34] Peng C, Wu H and Jiang X 2023 Nanotechnology-enabled ultrasound transducers *IEEE Nanotechnol. Mag.* **17** 4–12
[35] Muralt P, Polcawich R G and Trolier-McKinstry S 2009 Piezoelectric thin films for sensors, actuators, and energy harvesting *MRS Bull.* **34** 658–64
[36] Shaban M, Zayed M and Hamdy H 2017 Nanostructured ZnO thin films for self-cleaning applications *RSC Adv.* **7** 617–31
[37] Ito Y, Kushida K, Sugawara K and Takeuchi H 1995 A 100-MHz ultrasonic transducer array using ZnO thin films *IEEE Trans. Ultrason. Ferroelectr. Freq. Control* **42** 316–24

[38] Joshi B C and Chaudhri A K 2022 Sol–Gel-Derived Cu-Doped ZnO thin films for optoelectronic applications *ACS Omega* **7** 21877–81
[39] Ribut S H, Abdullah C A C and Yusoff M Z M 2019 Investigations of structural and optical properties of zinc oxide thin films growth on various substrates *Results Phys.* **13** 102146
[40] Sharma Y *et al* 2026 Recent advances in zinc oxide nanostructures: synthesis methods, doping Effects, Structural properties and emerging applications *Results Chem.* **25** 103227
[41] Duraccio D and Malucelli G 2026 ZnO micro- and nano-structures for the design of piezoelectric composites: recent advances in energy harvesting applications *Discov. Mater.* **6** 44
[42] Bhakyalatha M, Sathish S, Sekhar K C, Silva J P B and Kamakshi K 2025 ZnO nanostructures for biosensing applications: recent advances, challenges, and future perspectives *Microchem. J.* **213** 113893
[43] Maafa I M 2025 Potential of zinc oxide nanostructures in biosensor application *Biosensors* **15** 61
[44] Mohammed R Q and Ahmed B M 2025 Performance enhancement of ZnO/Zn nanostructure biosensor via cold atmosphere plasma *J. Nanopart. Res.* **27** 6
[45] Ciofani G *et al* 2010 Enhancement of neurite outgrowth in neuronal-like cells following boron nitride nanotube-mediated stimulation *ACS Nano* **4** 6267–77
[46] Jin C, Zhou J, Wu Z and Zhang J X J 2025 Doped zinc oxide-based piezoelectric devices for energy harvesting and sensing *Adv. Energy Sustain. Res.* **6** 2500017
[47] Kati N and Ayten B 2025 Investigation of structural and optical properties of boron-doped ZnO nanomaterials synthesized by hydrothermal method *J. Indian Chem. Soc.* **102** 101706
[48] Wang Z, Wang S, Lan B, Sun Y, Huang L, Ao Y, Li X, Jin L, Yang W and Deng W 2025 Piezotronic sensor for bimodal monitoring of achilles tendon behavior *Nanomicro. Lett.* **17** 241
[49] Güler A C, Dindar B and Örücü H 2019 Effect of B or N doping on the dielectric and electrical properties of ZnO at room temperature *Mater. Res. Express* **6** 065017
[50] Senol S D, Ozturk O and Terzioğlu C 2015 Effect of boron doping on the structural, optical and electrical properties of ZnO nanoparticles produced by the hydrothermal method *Ceram. Int.* **41** 11194–201
[51] Mao C, Fang L, Zhang H, Li W, Wu F, Qin G, Ruan H and Kong C 2016 Effect of B doping on optical, electrical properties and defects of ZnO films *J. Alloys Compd.* **676** 135–41
[52] Algün G, Alshater M and Akçay N 2024 Improved humidity sensing performances of boron doped ZnO nanostructured thin films depending on boron concentration *Phys. Scr.* **99** 055926
[53] Wang W, Ai T and Yu Q 2017 Electrical and photocatalytic properties of boron-doped ZnO nanostructure grown on PET–ITO flexible substrates by hydrothermal method *Sci. Rep.* **7** 42615
[54] Kim S, Park H, Nam G, Yoon H and Leem J-Y 2013 Improved optical and electrical properties of sol–gel-derived boron-doped zinc oxide thin films *J. Sol-Gel Sci. Technol.* **67** 580–91
[55] Kim S, Yoon H, Kim D Y, Kim S-O and Leem J-Y 2013 Optical properties and electrical resistivity of boron-doped ZnO thin films grown by sol–gel dip-coating method *Opt. Mater.* **35** 2418–24
[56] Kim S *et al* 2014 Hydrothermally grown boron-doped ZnO nanorods for various applications: structural, optical, and electrical properties *Electron. Mater. Lett.* **10** 81–87
[57] Ilican S, Yakuphanoglu F, Caglar M and Caglar Y 2011 The role of pH and boron doping on the characteristics of sol gel derived ZnO films *J. Alloys Compd.* **509** 5290–4
[58] Xi Y, Hu C G, Han X Y, Xiong Y F, Gao P X and Liu G B 2007 Hydrothermal synthesis of ZnO nanobelts and gas sensitivity property *Solid State Commun.* **141** 506–9
[59] Kathalingam A, Park H-C, Kim S-D, Kim H-S, Velumani S and Mahalingam T 2015 Synthesis of ZnO nanorods using different precursor solutions and their two terminal device characterization *J. Mater. Sci. Mater. Electron.* **26** 5724–34
[60] Dos Santos Silva W A, de Lima B S, Bernardi M I B and Mastelaro V R 2022 Enhancement of the ozone-sensing properties of ZnO through chemical-etched surface texturing *J. Nanopart. Res.* **24** 96
[61] Yadav S C and Uplane M D 2025 Synthesis and characterization of boron-doped ZnO thin films using a novel spray CVD Technique *Int. J. Sci. Res.* **14** 286–92
[62] Jang J *et al* 2015 A microelectromechanical system artificial basilar membrane based on a piezoelectric cantilever array and its characterization using an animal model *Sci. Rep.* **5** 12447
[63] Ilik B *et al* 2017 Thin Film PZT acoustic sensor for fully implantable cochlear implants *Proc. Eurosensors 2017, (Paris, France, 3–6 September 2017)* (MDPI) pp 366
[64] Baac H W, Ok J G, Maxwell A, Lee K-T, Chen Y-C, Hart A J, Xu Z, Yoon E and Guo L J 2012 Carbon-nanotube optoacoustic lens for focused ultrasound generation and high-precision targeted therapy *Sci. Rep.* **2** 989